A&A 407, 347–358 (2003)
DOI: 10.1051/0004-6361:20030880

Astronomy & Astrophysics

Are stellar coronae optically thin in X-rays?

A systematic investigation of opacity effects

J.-U. Ness[1], J. H. M. M. Schmitt[1], M. Audard[2], M. Güdel[3], and R. Mewe[4]

[1] Hamburger Sternwarte, Universität Hamburg, Gojenbergsweg 112, 21029 Hamburg, Germany
[2] Columbia Astrophysics Laboratory, 550 West 120th Street, New York, NY 10027, USA
[3] Paul Scherrer Institut, Würenlingen & Villigen, 5232 Villigen PSI, Switzerland
[4] National Institute for Space Research (SRON), Sorbonnelaan 2, 3584 CA Utrecht, The Netherlands

Received 23 January 2003 / Accepted 2 June 2003

Abstract. The relevance of resonant scattering in the solar corona has always been discussed controversially. Ratios of emission lines from identical ions but different oscillator strengths have been used in order to estimate damping of resonance lines due to possible resonant scattering, i.e., absorption by photo-excitation and re-emission out of the line of sight. The analysis of stellar spectra in analogy to previous works for the Sun is possible now with XMM-Newton and Chandra grating spectra and requires this issue to be considered again. In this work we present a sample of 45 X-ray spectra obtained for 26 stellar coronae with the RGS on board XMM-Newton and the LETGS and HETGS on board Chandra. We use ratios of the Fe XVII lines at 15.27 Å and 16.78 Å lines to the resonance line at 15.03 Å as well as the He-like f/r ratio of O VII and Ne IX to measure optical depth effects and compare them with ratios obtained from optically thin plasma atomic databases such as MEKAL, Chianti, and APEC. From the Fe XVII line ratios we find no convincing proof for resonance line scattering. Optical depths are basically identical for all kinds of stellar coronae and we conclude that identical optical depths are more probable when effects from resonant scattering are generally negligible. The 15.27/15.03 Å ratio shows a regular trend suggesting blending of the 15.27 Å line by a cooler Fe line, possibly Fe XVI. The He-like f/r ratios for O and Ne show no indication for significant damping of the resonance lines.
We mainly attribute deviations from the atomic databases to still uncertain emissivities which do not agree well with laboratory measurements and which come out with differing results when accounting for one or the other side effect. We attribute the discrepancies in the solar data to geometrical effects from observing individual emitting regions in the solar corona but only overall emission for stellar coronae including photons eventually scattered into the line of sight.

Key words. stars: activity – stars: coronae – stars: late type – X-rays: stars – atomic processes

1. Introduction

The emission line spectra obtained with the gratings on board the new X-ray observatories XMM-Newton and Chandra allow us to measure individual X-ray emission lines originating from ions in high ionization stages. These emission lines probe the hot tenuous plasma in stellar coronae. Obviously, the solar corona is much easier to study than stellar coronae, and observing techniques and methods originally developed for the analysis of the solar corona can now be applied to stellar coronae many years later with much improved technology. The theory required for X-ray spectroscopy developed in the 1960s and 70s now experiences a revival with the new generation of X-ray instruments applied to study stellar coronae.

The basic assumptions underlying almost all theoretical and observational analyses of solar and stellar coronal emission lines are, first, that the plasma is optically thin, and second, that the plasma is in collisional equilibrium. The latter implies that excitations are exclusively due to collisions and not to photo-excitation, the former implies that all photons produced in the hot plasma escape without further interaction. The plasma then cools through radiation (and possibly conduction). Radiative transport does not need to be considered, which makes the interpretation of coronal spectra and modeling of the coronal plasma much easier.

If this assumption were not true, opacity effects would first become visible in strong resonance lines. Resonance line photons could be absorbed and re-emitted in other directions. Depending on the plasma geometry, resonance line photons can be scattered out of the line of sight, but photons can also be scattered from other directions into the line of sight. Photons scattered back to the stellar surface will be absorbed rather than escape. Therefore, the line intensities of lines with strong scattering are reduced when compared to lines with no scattering.

Send offprint requests to: J.-U. Ness,
e-mail: jness@hs.uni-hamburg.de

This effect is called resonant scattering. In coronal equilibrium forbidden lines can always be considered optically thin because of their low radiative transition probabilities. Therefore the effect of resonant scattering can be recognized by resonance lines being damped in comparison to forbidden lines. Thus, the basic principle for detecting resonance scattering is to measure line flux ratios of definitely non-damped forbidden lines with low oscillator strengths f and resonance lines with high oscillator strengths. If this ratio is found to be enhanced compared to line ratios from theoretical predictions or from laboratory measurements, the resonance line should be considered optically thick. For a detailed account of the underlying theory we refer to Bahtia & Sabe (2001), Schmelz et al. (1997), Mariska (1992). We derive the reference line ratios from the line databases MEKAL[1] (Mewe et al. 1995), Chianti with ionization balances from Arnaud & Rothenflug (1985) (Dere et al. 2002; Young et al. 2003), and APEC[2] (e.g., Smith et al. 2001).

In the solar context the problem of resonant scattering of X-ray emission lines has been discussed with rather controversial conclusions. Acton & Catura (1976), Acton (1978), and Strong (1978) investigated the effects of resonant scattering for various He-like ions, especially the O VII resonance line at 21.6 Å. They found differences between theoretical and observed values of the temperature sensitive G-ratio $(f + i)/r$ (Gabriel & Jordan 1969) and interpreted these differences as being due to resonant scattering effects. Schmelz et al. (1997) and Saba et al. (1999) measured five different line ratios and found significant optical depths only for the Fe XVII line at 15.03 Å ($^1S_0 \rightarrow {}^1P_1$ with a high oscillator strength $f = 2.66$). They compared the 15.03 Å line flux with line flux measurements for Fe XVII lines with lower oscillator strengths, namely two intercombination lines $^1S_0 \rightarrow {}^3D_1$ at 15.27 Å with $f = 0.593$ and $^1S_0 \rightarrow {}^3P_1$ at 16.78 Å with $f = 0.1$. The different oscillator strengths indicate to which extent the transition can be subject to resonant scattering, i.e., the probability for resonant scattering of the 15.27 Å line is less than a quarter of that of the 15.03 Å line, while resonant scattering of the 16.78 Å line is even less probable, i.e., 0.04 times that for the 15.03 Å line. For the prediction of such line ratios for optically thin cases theory and experiment unfortunately do not agree with each other. The 15.27/15.03 Å line ratio has been measured in the Electron Beam Ion Trap (EBIT; Brown et al. 1998, 2001; Laming et al. 2000). These experiments typically yield Fe XVII 15.27/15.03 Å photon flux ratios in the range 0.3–0.36, which significantly differ from those expected from theoretical calculations. Also, Brown et al. (2001), Phillips et al. (1997) point out that contamination of the 15.27 Å line by an Fe XVI satellite line can further enhance the observed 15.27/15.03 Å photon flux ratio especially in cooler plasmas (below ~3 MK).

The optical thickness of stellar coronae has been investigated for EUV lines (e.g., Schrijver et al. 1994; Schmitt et al. 1996) measured with the Extreme Ultraviolet Explorer (EUVE). While Schrijver et al. (1994) claim to have found evidence for resonant scattering, Schmitt et al. (1996) argue using additional ROSAT observations that resonant scattering does not appear to be required for the interpretation of the EUV and X-ray spectra of inactive cool stars. From Chandra LETGS measurements Ness et al. (2001) ruled out optical depth effects in their analysis of Procyon and Capella. The assumption of a significant optical depth leads to unreasonably large emission measures contradicting their direct measurements of emission measures. Mewe et al. (2001) measured the Fe XVII 15.27/15.03 Å photon flux ratio for Capella of 0.35 ± 0.02 and derive a formal value of an optical depth τ (assuming slab geometries), which can be used in order to constrain loop lengths. The aspect of opacity effects has also been addressed for Capella by Phillips et al. (2001) using the same ratios and were found to be neglible. Ness et al. (2002b) measure the same ratio identical to the Capella measurement for the much more active star Algol. From this consistency they conclude that resonant scattering effects might in general be negligible for all coronae rather than being identical for all kinds of different coronae. This hypothesis is also supported by Audard et al. (2003) from an analysis of a sample of five active RS CVn stars, where also similar ratios are measured for all stars.

The purpose of this paper is a systematic investigation of potential optical depth effects in a large sample of stars covering a wide range of different activity levels. We will specifically analyze two Fe XVII line ratios and He-like f/r ratios for O VII and Ne IX for all cool stars, for which high-resolution spectra with the new X-ray instruments are available. We analyze 23 spectra obtained with the Reflection Grating Spectrometer (RGS) on board XMM-Newton, 12 spectra measured with the Low Energy Transmission Grating (LETGS) on board Chandra, and 10 spectra from the High Energy Transmission Grating (HETGS) on board Chandra (which are split in two spectra, the Medium Energy Grating (MEG) with a higher aperture and the High Energy Grating (HEG) with higher spectral resolution). Some stars have been measured by two or three instruments allowing comparison of calibration and/or finding variability of opacity effects. We will discuss possible trends and agreement and disagreement for measured line ratios with theoretical predictions. The major question we address is: Are resonant scattering effects dependent on the degree of activity, or are they negligible?

2. Reduction and analysis

2.1. Reduction of the raw data

For a most comprehensive analysis we studied line ratios relevant for detecting opacity effects from different instruments. From the XMM-Newton RGS GT program on board XMM-Newton, 23 spectra from stars in all stages of coronal activity are available. The reduction procedure for these data is identical for all spectra using SAS version 5.2. Five stars in our sample (RS CVn systems) have been described by Audard et al. (2003) and a detailed description of the reduction is given there. For some stars (47 Cas, AU Mic, κ Cet, and YZ CMi) we tested the effect of larger extraction regions comprising 95%

[1] Improved version; available at `http://www.sron.nl/divisions/hea/spex/version1.10/line/line_new.ps.gz`

[2] Version 1.2; available at `http://cxc.harvard.edu/atomdb`

Table 1. Properties of observed sample of 26 stars with 45 analysed spectra.

star	Spectr.	dist.	exposure time [ks]			$L_X(10^{28}$ erg/s)						
	type	[pc]	RGS1,2	LETG	HEG/	RGS1		RGS2		LETG	MEG	HEG
					MEG	1st order	2nd order	1st order	2nd order			
47 Cas[a]	F0.0Vn	33.56	50.66	–	–	112.88	161.85	184.34	122.27	–	–	–
AB Dor[b]	K1.0IIIp	14.94	58.87	–	52.33	70.87	50.96	65.81	44.72	–	73.87	58.21
α Cen A	G2V	1.34	–	81.50	–	–	–	–	–	0.08	–	–
α Cen B	K0V	1.34	7.04	81.50	–	–	–	–	–	0.07	–	–
AD Leo	M3.5V	4.70	36.25	48.50	–	3.50	3.01	3.07	2.03	3.93	–	–
Algol	B8.0V/K2.0III	28.00	52.66	81.40	51.73	283.73	–	–	–	944.99	673.63	557.72
AR Lac	G2.0IV	42.03	32.10	–	32.09	627.14	612.06	730.55	464.23	–	514.49	415.12
AT Mic	M4.4	10.22	28.19	–	–	15.47	14.44	20.49	11.46	–	–	–
AU Mic[a]	M0.0	9.94	55.74	–	58.81	12.43	14.42	18.31	10.53	–	11.52	8.55
β Cet	K0.0III	29.38	13.02	108.04	86.06	198.67	320.16	328.04	256.10	699.24	253.19	227.48
Capella[b]	G5.0IIIe	12.94	52.92	218.50	154.68	145.38	157.22	168.06	132.10	186.56	153.08	127.43
χ^1 Ori	G0.0V	8.66	29.96	–	–	6.21	6.14	4.95	4.09	–	–	–
EK Dra	F8.0	33.94	34.31	67.24	–	61.25	72.78	97.76	54.54	85.01	–	–
ϵ Eri	K2.0V	3.22	13.34	108.00	–	0.55	0.55	–	0.53	1.53	–	–
EQ Peg[b]	M3.5	6.25	15.52	–	–	4.31	3.48	3.81	2.80	–	–	–
EV Lac	M3.5	5.05	32.71	–	100.06	3.58	2.97	4.03	2.11	–	2.86	2.19
HR 1099	G9.0V	28.97	26.27	97.50	94.68	432.49	384.98	488.85	313.58	973.74	1000.85	798.38
κ Cet[a]	G5.0Vvar	9.16	39.95	–	–	5.61	5.27	2.79	3.44	–	–	–
λ And	G8.0III	25.81	31.83	–	81.91	249.61	238.61	295.03	188.31	–	198.33	121.17
π^1 UMa	G1.5Vb	14.27	52.90	–	–	2.56	6.19	5.13	4.14	7.29	–	–
Procyon	F5.0IV-V	3.50	–	140.70	–	–	–	–	–	0.49	–	–
σ CrB	G0.0	21.70	19.31	–	–	322.59	338.72	307.83	312.74	–	–	–
UX Ari	G5.0IV	50.23	30.91	112.76	48.47	953.03	873.75	1059.84	691.82	1306.36	804.46	502.40
VY Ari	K0.0	43.99	33.82	–	–	366.79	352.07	460.52	266.27	–	–	–
YY Gem	M0.5V	15.80	–	59.00	–	–	–	–	–	37.12	–	–
YZ CMi[a]	M4.5V:e	5.93	27.24	–	–	3.30	1.59	3.07	1.94	–	–	–

[a] RGS spectra with 95% extraction regions.
[b] Full RGS1 range available.

source photons (instead of 90%), but find no significant improvement. Three observations (AB Dor, Capella, and EQ Peg) have been carried out before the chip failure on the RGS1, so that the range between 10.5 and 13.8 Å is available also with the RGS1 for these stars. The analysis of Ne IX is still not possible with the RGS1 for these stars, because of bad pixels on the chip where the photons from the 13.7 Å (the Ne IX forbidden line) are extracted. Line counts are measured with the CORA program (Sect. 2.2) and the ASCII files required for CORA were produced with XSPEC from the fits files returned by the SAS software. From the response matrices effective areas were calculated and stored in ASCII files which are used as look-up tables for converting measured line counts into line fluxes.

Most of the LETGS data included have been introduced by Ness et al. (2002a) and for details on the data reduction we refer to that paper (effective areas from Deron Pease, Aug. 2002). We also analyze HETGS spectra of all cool stars available to us and use the pre-processed pha files from the Chandra archive. In Table 1 we list specifications for 45 observations of 26 stars with exposure times and X-ray luminosities obtained from the different instruments. We summed all first order photons converted to energy fluxes using the effective areas, exposure times and distances in order to calculate X-ray luminosities. Differences in X-ray luminosities by no more than a factor of two occur, although they are extracted in the same wavelength intervals (except for MEG and HEG, which are extracted in their complete wavelength ranges), because photons in the chip gaps on RGS1 and RGS2 are missing and higher order photons in the LETGS are not corrected for.

2.2. Measurement of line fluxes

Line counts are measured with a modified version of the CORA program by Ness & Wichmann (2002). Due to small count numbers all spectra in our sample require Poisson statistics to be applied. Since the conventional background subtraction ruins the Poissonian statistics, we construct a model spectrum consisting of the sum of three components. The line spectrum is modeled with analytical line profile functions representing instrumental point spread functions (Lorentzian for the RGS spectra, Gaussian for the MEG and HEG spectra and a "β model" for the LETGS spectra, which is a Lorentzian with an exponent $\beta = 2.5$). The background is split in two components, the instrumental background (extracted from regions on the detectors adjacent to the dispersion directions) and a source continuum (modeled as a constant value representing a number of counts per bin over the wavelength region under individual consideration). The sum of these three components is compared to the non-subtracted spectrum in order to calculate likelihood values to be minimized. The modeling is restricted only to the line parameters' position, line width and line counts, but the two background components must be given a priori (cf. Sect. 2.3). Therefore the errors (1σ errors) given for the line counts represent only statistical errors (including correlated

errors from possible line blends), but systematic uncertainties from the placement of a continuum value are not included.

2.3. Placement of the continuum

The accuracy of the iterated line model clearly depends on the choice of the two background components. The instrumental background is no problem, because it can be measured from adjacent regions on the detector plates. However, the determination of reliable source continua (comprising true continuum and pseudo continuum of unresolved weak lines) is much more difficult. We consider the source continuum to be constant over small wavelength regions (small range including the emission lines to be measured) and assign a single source background parameter *sbg* in units counts/Å to represent this flat source continuum. In the CORA program such a value for a source continuum can be specified directly by hand or the median value of all bins in the wavelength region covering the lines under consideration can be selected, which is only valid as long as less than 50% of the bins belong to emission lines. All bins containing count numbers higher than 3σ above this median value ($\sigma = \sqrt{\text{median}}$) are regarded to obviously belong to emission lines and are excluded from calculating the final *sbg* median value.

The specific challenge posed by RGS spectra is that the line wings are broad and overlap. The inclusion of correlated statistical errors is thus very important, but the determination of an adequate value for the source background is more difficult. The median value will systematically overestimate the source continuum, because more bins belong to the emission lines rather than representing the source continuum and line counts will then be underestimated. For the purpose of this paper, the Fe XVII lines around 15 Å are measured, and this wavelength region contains many nearby lines, such that for the median calculation only small regions representing the continuum are available.

We therefore modified the program to calculate a value for the source background by refining the median calculation. The 3σ criterion is already an attempt to remove some bins that belong to emission lines in order to increase the percentage of remaining bins belonging to the background. For our purpose we modify this criterion in two ways. First, the removal of bins with high count numbers and the calculation of a new median value are repeated iteratively until no more bins contain more counts than 3σ above the respective median values. Secondly, a new parameter n_σ is introduced. In this way median values are iteratively calculated after removal of all bins with count values higher than $n_\sigma \times \sigma$, i.e., $\text{median}_{\text{new}} = \text{median}(\text{bins} < n_\sigma \times \sqrt{\text{median}_{\text{last}}})$. Small values of n_σ will more critically remove high-count bins resulting in lower source background values. Usage of this parameter represents a parameterized choice of source continuum values by eye.

In Fig. 1 we show the 15 Å region of λ And with attempts to obtain a most realistic source background value using the new parameter. It can be seen that this wavelength region is full of emission lines and that significantly more than 50% of all bins belong to emission lines rather than the background emission.

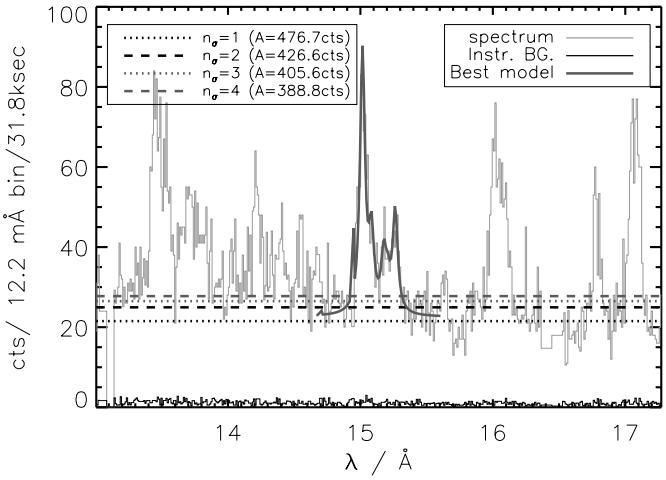

Fig. 1. 15 Å region of λ And with RGS2. Placement of a constant source continuum with median values using different parameters n_σ. The respective counts resulting from the different choices of n_σ are given in the upper left. The best model with four lines is obtained for $n_\sigma = 1$ and is overplotted with dark grey. An overestimated continuum value leads to systematically underestimated 15.27/15.03 Å line count ratios hiding possible resonant scattering effects.

By gradually reducing n_σ the median background can significantly be reduced, and with $n_\sigma = 1$ a most suitable background is found. The resulting count number for the 15.03 Å line ranges from 388.8 to 476.7 counts. This demonstrates that systematic errors of order 25% must be added to the given statistical errors. In the following we use $n_\sigma = 1$ for all spectra when fitting the 15 Å lines and $n_\sigma = 1.5$ for the 16.78 Å line. The neon and oxygen lines are all measured with the old method.

2.4. Measured line counts

Since in the RGS1 bad pixels corrupt the measurement of the 15.27 Å line we analyze only the RGS2 data and the LETGS, MEG, and HEG data for the iron measurements. The He-like lines were measured with RGS1, LETGS, and MEG (oxygen) and with RGS2, LETGS, MEG, and HEG (neon).

The fit results for the three Fe XVII lines at 15.03 Å, 15.27 Å, and at 16.78 Å are listed in Table 2. These counts are converted to energy fluxes in order to derive line flux ratios using effective areas obtained from the response matrices for comparison with line flux ratios from the databases MEKAL, Chianti, and APEC, which all list optically thin emissivities for given temperature grids. The results for the measured ratios are also listed in Table 2.

The line counts measured for the He-like f and r lines of O VII and Ne IX are listed in Tables 3 and 4, respectively. We also measure the O VIII Ly$_\alpha$ line, and from the O VIII Ly$_\alpha$/O VII r line ratios we assign a characteristic coronal temperature to each star (using the APEC line database). Further, we calculate X-ray luminosities emitted in all three He-like lines (r, i, and f summed) as activity indicators (cf. Fig. 2). In addition to the line counts for oxygen we list the

Table 2. Measured line counts for Fe XVII lines with 1 σ errors.

		Fe XVII			Ratios		
star	Instr.	15.03 Å	15.27 Å	16.78 Å	15.27/15.03 Å	16.78/15.03 Å	15.27/16.78 Å
47 Cas	RGS2	506.28 ± 32.80	215.94 ± 25.97	419.17 ± 26.64	0.40 ± 0.05	0.77 ± 0.07	0.52 ± 0.07
AB Dor	RGS2	1132.6 ± 48.68	464.77 ± 39.14	905.31 ± 40.05	0.39 ± 0.03	0.74 ± 0.04	0.52 ± 0.05
	MEG	538.89 ± 24.37	203.40 ± 15.96	241.83 ± 16.35	0.39 ± 0.03	0.59 ± 0.04	0.66 ± 0.06
	HEG	91.010 ± 9.892	37.030 ± 6.595	18.580 ± 4.359	0.43 ± 0.09	0.62 ± 0.16	0.70 ± 0.20
AD Leo	RGS2	429.66 ± 29.84	159.63 ± 23.61	380.81 ± 24.73	0.35 ± 0.05	0.82 ± 0.07	0.42 ± 0.06
	LETG	313.64 ± 20.17	133.11 ± 15.45	189.05 ± 15.70	0.41 ± 0.05	0.53 ± 0.05	0.77 ± 0.11
Algol	RGS2	1028.4 ± 49.94	457.75 ± 40.60	684.78 ± 39.29	0.42 ± 0.04	0.62 ± 0.04	0.68 ± 0.07
	LETG	1134.5 ± 42.19	378.77 ± 31.01	698.16 ± 33.95	0.32 ± 0.02	0.54 ± 0.03	0.59 ± 0.05
	MEG	621.70 ± 27.55	226.82 ± 18.68	294.40 ± 19.00	0.38 ± 0.03	0.62 ± 0.04	0.61 ± 0.06
	HEG	104.25 ± 10.66	39.750 ± 6.837	13.140 ± 3.780	0.41 ± 0.08	0.38 ± 0.11	1.07 ± 0.35
AR Lac	RGS2	582.06 ± 35.42	259.47 ± 29.81	390.62 ± 28.58	0.42 ± 0.05	0.62 ± 0.06	0.67 ± 0.09
	MEG	218.91 ± 15.85	79.000 ± 10.28	107.15 ± 10.98	0.37 ± 0.05	0.64 ± 0.08	0.58 ± 0.09
AT Mic	RGS2	294.34 ± 24.58	88.730 ± 18.89	213.98 ± 19.77	0.28 ± 0.06	0.68 ± 0.08	0.42 ± 0.09
AU Mic	RGS2	857.76 ± 40.54	336.14 ± 31.18	477.49 ± 28.79	0.37 ± 0.03	0.52 ± 0.04	0.71 ± 0.07
	MEG	217.18 ± 15.51	78.240 ± 9.768	90.760 ± 10.07	0.37 ± 0.05	0.55 ± 0.07	0.68 ± 0.11
	HEG	28.080 ± 5.613	7.6600 ± 3.173	6.9400 ± 2.646	0.29 ± 0.13	0.75 ± 0.32	0.39 ± 0.22
β Cet	RGS2	752.18 ± 40.03	286.31 ± 26.32	619.54 ± 30.46	0.36 ± 0.03	0.77 ± 0.05	0.47 ± 0.04
	LETG	3718.0 ± 70.06	1248.1 ± 45.71	2008.5 ± 50.64	0.32 ± 0.01	0.48 ± 0.01	0.68 ± 0.03
	MEG	1954.0 ± 45.23	672.90 ± 27.24	827.40 ± 29.22	0.36 ± 0.01	0.56 ± 0.02	0.64 ± 0.03
	HEG	298.67 ± 17.44	108.19 ± 10.61	50.690 ± 7.141	0.39 ± 0.04	0.51 ± 0.07	0.75 ± 0.13
Capella	RGS2	11967. ± 145.8	5284.1 ± 110.5	9436.1 ± 117.3	0.42 ± 0.01	0.73 ± 0.01	0.57 ± 0.01
	LETG	22759. ± 165.8	8940.5 ± 111.5	14024. ± 124.6	0.38 ± 0.01	0.54 ± 0.01	0.69 ± 0.01
	MEG	14047. ± 120.8	5343.9 ± 76.05	6629.4 ± 82.34	0.40 ± 0.01	0.62 ± 0.01	0.64 ± 0.01
	HEG	2712.3 ± 52.65	843.36 ± 29.72	503.93 ± 22.52	0.33 ± 0.01	0.56 ± 0.02	0.59 ± 0.03
χ^1 Ori	RGS2	549.96 ± 30.83	265.64 ± 24.36	404.77 ± 24.20	0.46 ± 0.04	0.68 ± 0.05	0.66 ± 0.07
EK Dra	RGS2	280.71 ± 22.36	54.790 ± 14.60	210.94 ± 17.96	0.18 ± 0.05	0.70 ± 0.08	0.26 ± 0.07
	LETG	204.32 ± 16.49	65.458 ± 10.53	102.86 ± 12.91	0.31 ± 0.05	0.44 ± 0.06	0.69 ± 0.14
ϵ Eri	RGS2	230.74 ± 19.67	123.29 ± 16.27	185.60 ± 16.44	0.50 ± 0.08	0.75 ± 0.09	0.67 ± 0.10
	LETG	1054.9 ± 34.98	462.69 ± 24.38	739.58 ± 28.96	0.42 ± 0.02	0.62 ± 0.03	0.68 ± 0.04
EQ Peg	RGS2	134.74 ± 16.70	59.830 ± 13.14	123.28 ± 14.43	0.42 ± 0.10	0.85 ± 0.14	0.49 ± 0.12
EV Lac	RGS2	403.93 ± 28.68	154.06 ± 20.51	292.15 ± 22.44	0.36 ± 0.05	0.67 ± 0.07	0.53 ± 0.08
	MEG	333.57 ± 18.93	183.79 ± 14.40	180.05 ± 13.84	0.57 ± 0.05	0.71 ± 0.06	0.81 ± 0.08
	HEG	62.580 ± 8.187	20.190 ± 4.849	10.800 ± 3.313	0.34 ± 0.09	0.52 ± 0.17	0.66 ± 0.25
HR 1099	RGS2	553.53 ± 37.37	222.57 ± 30.33	337.93 ± 29.10	0.38 ± 0.05	0.57 ± 0.06	0.67 ± 0.10
	LETG	1204.3 ± 42.48	434.95 ± 31.77	728.82 ± 36.98	0.35 ± 0.02	0.54 ± 0.03	0.65 ± 0.05
	MEG	1227.7 ± 39.05	445.89 ± 26.59	644.34 ± 28.31	0.38 ± 0.02	0.69 ± 0.03	0.54 ± 0.04
	HEG	240.44 ± 16.57	72.760 ± 10.13	43.570 ± 7.306	0.32 ± 0.05	0.55 ± 0.10	0.59 ± 0.12
κ Cet	RGS2	550.57 ± 31.34	312.80 ± 27.04	619.60 ± 29.86	0.53 ± 0.05	1.05 ± 0.07	0.51 ± 0.05
λ And	RGS2	478.78 ± 33.93	197.61 ± 28.29	336.44 ± 28.02	0.39 ± 0.06	0.65 ± 0.07	0.59 ± 0.09
	MEG	558.06 ± 25.05	201.97 ± 16.07	241.32 ± 16.13	0.38 ± 0.03	0.57 ± 0.04	0.66 ± 0.06
	HEG	58.620 ± 7.790	23.100 ± 4.943	–	0.42 ± 0.10	–	–
π^1 UMa	RGS2	450.19 ± 27.04	176.91 ± 21.40	323.24 ± 21.57	0.37 ± 0.05	0.67 ± 0.06	0.55 ± 0.07
Procyon	LETG	101.56 ± 13.37	38.450 ± 10.07	59.030 ± 11.56	0.37 ± 0.10	0.51 ± 0.12	0.71 ± 0.23
σ CrB	RGS2	1626.6 ± 56.60	673.04 ± 41.30	1009.9 ± 40.78	0.39 ± 0.02	0.58 ± 0.03	0.67 ± 0.05
UX Ari	RGS2	220.17 ± 27.35	73.050 ± 20.96	211.92 ± 24.48	0.31 ± 0.09	0.90 ± 0.15	0.35 ± 0.10
	LETG	497.87 ± 29.79	151.85 ± 22.32	277.58 ± 23.61	0.29 ± 0.04	0.49 ± 0.05	0.59 ± 0.10
	MEG	219.83 ± 16.26	79.050 ± 10.85	92.730 ± 10.55	0.37 ± 0.05	0.55 ± 0.07	0.67 ± 0.12
VY Ari	RGS2	291.14 ± 26.33	90.040 ± 20.14	161.97 ± 19.96	0.29 ± 0.07	0.52 ± 0.08	0.56 ± 0.14
YY Gem	LETG	252.48 ± 18.17	92.900 ± 12.66	139.56 ± 14.36	0.35 ± 0.05	0.49 ± 0.06	0.72 ± 0.12
YZ CMi	RGS2	163.75 ± 18.27	97.110 ± 16.44	145.15 ± 15.44	0.56 ± 0.11	0.82 ± 0.12	0.67 ± 0.13

derived temperatures and O VII and Ne IX luminosities in Tables 3 and 4. The plasma temperature is also a good activity indicator (Güdel et al. 1997).

3. Results

The measured line fluxes are used in order to plot the line ratios sensitive to resonant scattering versus activity indicators, i.e., temperatures for the Fe XVII ratios and X-ray luminosities contained in the He-like lines for the f/r ratios of O VII and Ne IX.

3.1. Fe XVII line ratios

In Fig. 3 we plot the Fe XVII line ratios of 15.27/15.03 Å lines and for 16.78/15.03 Å lines from Table 2 versus O VIII/O VII characteristic temperatures used as activity indicators (listed in Table 3). The horizontal lines represent theoretical low-optical depth ratios as a function of temperature predicted by interpolation from MEKAL, APEC, and Chianti, respectively. For the 16.78/15.03 Å line ratios we also included new theoretical predictions by Doron & Behar (2002), who account for dielectronic and radiative

Table 3. Measured line counts for O VII resonance (r) and forbidden (f) lines and O VIII (Ly_α), O VII luminosities L_{OVII}, and O VIII/O VII temperatures.

star	Instr.	r	f	f/r	$\log(L_{OVII})^a$	Ly_α	T^b/MK
47 Cas	RGS1	186.55 ± 18.08	105.41 ± 14.67	0.565 ± 0.09	28.25 ± 0.06	1275.7 ± 39.89	4.73 ± 0.22
AB Dor	RGS1	788.24 ± 35.68	407.50 ± 27.21	0.517 ± 0.04	28.12 ± 0.02	3760.9 ± 68.54	4.12 ± 0.06
	MEG	44.570 ± 7.304	36.980 ± 6.752	0.829 ± 0.20	27.93 ± 0.09	814.23 ± 28.94	5.88 ± 0.49
α Cen A	LETG	138.26 ± 12.31	109.60 ± 11.06	0.792 ± 0.10	25.65 ± 0.04	60.890 ± 8.748	1.88 ± 0.08
α Cen B	RGS1	157.81 ± 13.96	111.23 ± 11.60	0.704 ± 0.09	26.26 ± 0.05	188.22 ± 14.73	2.60 ± 0.07
	LETG	160.32 ± 13.35	154.54 ± 13.06	0.963 ± 0.11	25.74 ± 0.04	130.31 ± 12.45	2.16 ± 0.06
AD Leo	RGS1	705.13 ± 30.13	356.13 ± 22.02	0.505 ± 0.03	27.26 ± 0.02	2132.8 ± 49.62	3.47 ± 0.05
	LETG	263.97 ± 17.47	170.31 ± 14.52	0.645 ± 0.07	27.19 ± 0.03	1238.4 ± 36.40	3.64 ± 0.10
Algol	LETG	262.49 ± 22.60	120.90 ± 18.00	0.460 ± 0.07	28.54 ± 0.05	2883.0 ± 57.81	5.11 ± 0.17
	MEG	71.410 ± 9.874	31.580 ± 7.295	0.442 ± 0.11	28.67 ± 0.08	627.34 ± 26.08	4.32 ± 0.23
AR Lac	RGS1	184.05 ± 20.00	110.15 ± 16.82	0.598 ± 0.11	28.66 ± 0.07	1523.8 ± 45.25	5.14 ± 0.23
	MEG	16.430 ± 4.716	3.8000 ± 2.859	0.231 ± 0.18	28.37 ± 0.28	247.82 ± 16.18	5.40 ± 0.76
AT Mic	RGS1	501.50 ± 26.17	238.57 ± 18.83	0.475 ± 0.04	27.90 ± 0.03	1603.7 ± 43.38	3.53 ± 0.07
AU Mic	RGS1	944.27 ± 36.41	688.37 ± 31.28	0.729 ± 0.04	27.88 ± 0.02	3224.4 ± 61.78	3.62 ± 0.05
	MEG	53.790 ± 7.523	45.990 ± 6.974	0.855 ± 0.17	27.58 ± 0.07	454.11 ± 21.41	4.26 ± 0.22
β Cet	RGS1	128.24 ± 14.40	79.437 ± 11.74	0.619 ± 0.11	28.56 ± 0.07	561.27 ± 26.51	4.01 ± 0.18
	LETG	241.35 ± 21.66	178.69 ± 20.17	0.740 ± 0.10	28.43 ± 0.05	2176.2 ± 50.82	4.68 ± 0.20
	MEG	47.120 ± 7.198	23.610 ± 5.252	0.501 ± 0.13	28.19 ± 0.10	548.17 ± 23.72	4.87 ± 0.34
Capella	RGS1	2611.2 ± 60.23	1520.5 ± 46.65	0.582 ± 0.02	28.53 ± 0.01	7272.0 ± 94.37	3.37 ± 0.02
	LETG	3071.2 ± 56.00	2135.2 ± 51.10	0.695 ± 0.02	28.49 ± 0.01	14677. ± 124.3	3.67 ± 0.02
χ^1 Ori	RGS1	184.68 ± 16.02	123.42 ± 13.40	0.668 ± 0.09	27.30 ± 0.05	490.75 ± 24.35	3.33 ± 0.09
EK Dra	RGS1	86.306 ± 11.43	59.680 ± 9.822	0.691 ± 0.14	28.16 ± 0.07	409.05 ± 22.60	4.11 ± 0.21
	LETG	53.253 ± 9.516	31.025 ± 7.533	0.582 ± 0.17	28.12 ± 0.11	324.56 ± 19.49	4.04 ± 0.29
ϵ Eri	RGS1	217.64 ± 16.47	160.21 ± 14.34	0.736 ± 0.08	26.90 ± 0.04	482.75 ± 23.73	3.17 ± 0.09
	LETG	697.02 ± 27.70	453.99 ± 22.78	0.651 ± 0.04	26.95 ± 0.02	2025.8 ± 46.07	3.13 ± 0.05
EQ Peg	RGS1	273.77 ± 19.17	142.72 ± 13.99	0.521 ± 0.06	27.45 ± 0.04	717.49 ± 28.77	3.31 ± 0.07
EV Lac	RGS1	471.98 ± 25.54	291.00 ± 20.31	0.616 ± 0.05	27.23 ± 0.03	1526.2 ± 42.31	3.55 ± 0.07
	MEG	119.25 ± 11.12	54.920 ± 7.585	0.460 ± 0.07	27.04 ± 0.05	694.39 ± 26.61	3.71 ± 0.15
HR 1099	RGS1	357.12 ± 26.86	254.27 ± 23.89	0.712 ± 0.08	28.73 ± 0.04	2164.1 ± 53.29	4.49 ± 0.14
	LETG	470.60 ± 27.82	254.79 ± 22.49	0.541 ± 0.05	28.71 ± 0.03	5584.1 ± 78.60	5.25 ± 0.12
	MEG	207.77 ± 16.12	93.870 ± 11.80	0.451 ± 0.06	28.78 ± 0.05	2867.9 ± 54.95	5.21 ± 0.15
κ Cet	RGS1	236.88 ± 18.54	153.99 ± 15.00	0.650 ± 0.08	27.34 ± 0.04	632.93 ± 27.79	3.33 ± 0.09
λ And	RGS1	264.86 ± 22.73	131.08 ± 17.88	0.494 ± 0.08	28.34 ± 0.06	1959.8 ± 50.39	4.92 ± 0.20
	MEG	74.030 ± 9.337	33.550 ± 6.642	0.453 ± 0.10	28.29 ± 0.08	919.35 ± 30.80	5.02 ± 0.28
π^1 UMa	RGS1	134.95 ± 13.36	94.810 ± 11.76	0.702 ± 0.11	27.39 ± 0.06	383.45 ± 21.96	3.40 ± 0.12
Procyon	LETG	731.60 ± 28.70	652.40 ± 27.40	0.891 ± 0.05	26.99 ± 0.02	673.20 ± 27.60	2.22 ± 0.03
σ CrB	RGS1	311.61 ± 24.22	173.44 ± 20.53	0.556 ± 0.07	28.51 ± 0.05	2016.1 ± 51.28	4.62 ± 0.16
UX Ari	RGS1	245.26 ± 23.32	117.54 ± 18.79	0.479 ± 0.08	28.89 ± 0.06	2173.7 ± 52.95	5.27 ± 0.20
	LETG	300.35 ± 22.37	227.42 ± 20.40	0.757 ± 0.08	28.96 ± 0.04	3321.1 ± 61.27	5.12 ± 0.14
	MEG	52.410 ± 7.733	20.910 ± 5.421	0.399 ± 0.11	28.92 ± 0.10	524.68 ± 23.26	4.55 ± 0.30
VY Ari	RGS1	205.56 ± 19.97	144.81 ± 17.34	0.704 ± 0.10	28.75 ± 0.06	1314.6 ± 40.65	4.59 ± 0.20
YY Gem	LETG	193.31 ± 15.47	115.75 ± 12.44	0.598 ± 0.08	28.03 ± 0.04	971.47 ± 32.27	3.74 ± 0.13
YZ CMi	RGS1	287.29 ± 19.46	169.54 ± 15.80	0.590 ± 0.06	27.21 ± 0.04	807.37 ± 30.60	3.38 ± 0.08

[a] In erg/s.
[b] From O VIII/O VII (Ly_α/r) ratio with APEC.

recombination from Fe XVIII, inner-shell ionization from Fe XVI, and resonant excitation through doubly excited levels of Fe XVI (3-ion model) in their calculations. The model predictions lie significantly higher than the predictions from the other databases, but their 1-ion model and their predictions for the 15.27/15.03 Å line ratio are consistent with the other predictions.

Comparing our measurements of the 15.27/15.03 Å line ratios with the theoretical predictions the measured ratios are systematically higher than predicted with no apparent correlation with temperature except possibly for the coolest coronae in our sample where the ratios are highest. For the 16.78/15.03 Å ratios we find no correlation with temperature at all, but a larger scatter with systematic deviations from the databases, although good agreement with the predictions by Doron & Behar (2002) is seen.

In Fig. 4 we plot only the LETGS and MEG measurements, where the scatter due to systematic and statistical uncertainties is much smaller. The reason is that the RGS ratios suffer from systematic uncertainties in the placement of the source continuum (due to broad line wings; cf. Sect. 2.3) and the HEG measurements have low signal to noise and have thus large statistical uncertainties. In the left panel of Fig. 4 it can be seen that the 15.27/15.03 Å ratio is remarkably constant for all sources except for the MEG measurement of EV Lac, which deviates considerably from all the other MEG and LETGS measurements; this data point is marked by a filled triangle. Both Fe XVII ratios thus suggest that resonant scattering plays a

Table 4. Measured line counts for Ne IX resonance (r) and forbidden (f) lines and Ne IX luminosities $L_{\rm Ne\,IX}$ from summed ($r + i + f$) line fluxes.

star	Instr.	r	f	$\log(L_{\rm Ne\,IX})^a$
47 Cas	RGS2	452.00 ± 38.77	278.85 ± 28.22	28.64 ± 0.04
AB Dor	RGS2	1614.6 ± 57.63	1030.0 ± 50.39	28.45 ± 0.01
	MEG	524.16 ± 26.51	290.84 ± 18.73	28.34 ± 0.02
	HEG	110.99 ± 10.98	77.682 ± 9.189	28.33 ± 0.05
AD Leo	RGS2	553.77 ± 37.81	400.75 ± 29.26	27.22 ± 0.03
	LETG	276.32 ± 19.20	165.42 ± 16.04	27.16 ± 0.04
Algol	LETG	631.23 ± 36.62	347.91 ± 31.94	28.83 ± 0.04
	MEG	283.27 ± 23.00	194.68 ± 18.40	28.65 ± 0.04
	HEG	79.109 ± 9.973	57.690 ± 8.389	28.79 ± 0.06
AR Lac	RGS2	488.50 ± 42.06	364.31 ± 33.39	29.12 ± 0.04
	MEG	152.66 ± 14.84	136.82 ± 13.30	29.00 ± 0.05
	HEG	39.833 ± 6.650	15.984 ± 4.306	28.93 ± 0.10
AT Mic	RGS2	632.39 ± 34.03	387.00 ± 28.22	28.03 ± 0.02
AU Mic	RGS2	1156.9 ± 45.71	812.28 ± 41.49	27.97 ± 0.02
	MEG	319.98 ± 19.79	212.47 ± 15.78	27.74 ± 0.03
	HEG	87.094 ± 9.526	52.332 ± 7.293	27.80 ± 0.06
β Cet	LETG	679.75 ± 41.78	465.82 ± 35.45	28.78 ± 0.03
	MEG	363.20 ± 23.78	211.92 ± 17.14	28.58 ± 0.03
	HEG	82.103 ± 9.361	64.720 ± 8.301	28.61 ± 0.06
Capella	LETG	3960.8 ± 79.78	2312.8 ± 66.94	28.58 ± 0.01
	MEG	2512.9 ± 60.13	1373.2 ± 42.87	28.43 ± 0.01
	HEG	616.43 ± 25.70	373.48 ± 20.09	28.46 ± 0.02
EK Dra	RGS2	172.87 ± 20.22	139.63 ± 18.39	28.47 ± 0.05
ϵ Eri	RGS2	213.28 ± 19.03	125.74 ± 16.75	26.87 ± 0.04
	LETG	564.02 ± 27.20	347.98 ± 22.35	26.82 ± 0.02
EQ Peg	RGS2	209.59 ± 23.72	154.66 ± 18.08	27.41 ± 0.05
EV Lac	RGS2	376.34 ± 31.23	253.93 ± 24.17	27.14 ± 0.04
	MEG	454.53 ± 23.74	222.32 ± 16.34	27.02 ± 0.03
	HEG	115.34 ± 11.01	68.823 ± 8.547	27.08 ± 0.05
HR 1099	RGS2	762.77 ± 44.32	409.12 ± 36.44	29.03 ± 0.03
	LETG	1231.7 ± 45.61	727.60 ± 39.44	29.09 ± 0.02
	MEG	1690.5 ± 50.43	834.17 ± 34.81	29.13 ± 0.01
	HEG	477.47 ± 22.85	228.75 ± 16.25	29.21 ± 0.02
κ Cet	RGS2	251.60 ± 23.27	193.82 ± 21.53	27.40 ± 0.04
λ And	RGS2	532.86 ± 39.36	335.00 ± 33.78	28.71 ± 0.03
	MEG	506.89 ± 26.09	219.34 ± 17.80	28.55 ± 0.03
	HEG	54.933 ± 7.704	35.636 ± 6.216	28.28 ± 0.08
π^1 UMa	RGS2	158.38 ± 19.24	105.83 ± 15.87	27.46 ± 0.06
Procyon	LETG	66.930 ± 10.46	35.030 ± 8.468	25.83 ± 0.10
σ CrB	RGS2	693.59 ± 48.82	344.81 ± 37.72	28.86 ± 0.03
UX Ari	RGS2	671.37 ± 40.05	456.80 ± 33.42	29.42 ± 0.02
	LETG	564.02 ± 27.20	347.98 ± 22.35	29.19 ± 0.02
	MEG	409.21 ± 23.32	237.38 ± 17.32	29.33 ± 0.03
	HEG	48.597 ± 7.493	18.571 ± 4.596	28.95 ± 0.10
VY Ari	RGS2	481.21 ± 33.86	306.33 ± 28.95	29.11 ± 0.03
YY Gem	LETG	240.53 ± 18.54	137.45 ± 15.34	28.06 ± 0.05
YZ CMi	RGS2	195.54 ± 22.57	101.04 ± 15.84	27.01 ± 0.06

[a] In erg/s.

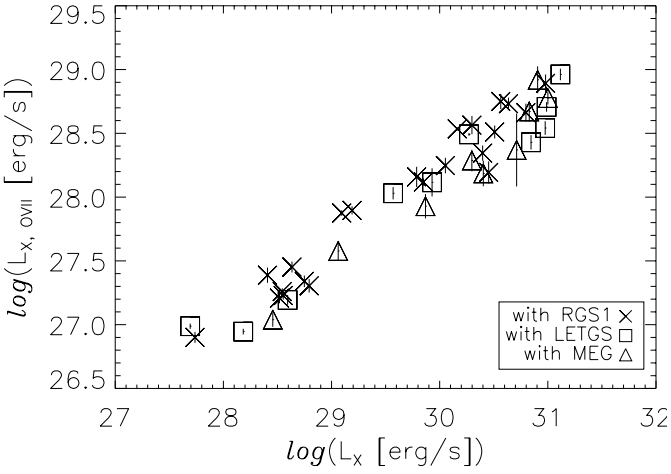

Fig. 2. O VII line fluxes converted to luminosities compared to total X-ray luminosities: The O VII-luminosities are representative as activity indicators.

significant role for EV Lac, however, this high ratio cannot be confirmed in the simultaneous HEG measurement nor in the RGS2 data. We show the two spectra obtained with MEG and RGS2 for EV Lac in Fig. 7, where the different ratios can be recognized.

In order to compare our measurements with solar measurements we include the solar measurements from Saba et al. (1999) in the form of shaded areas in Figs. 3 and 4. They deduced significant optical depths for the 15.03 Å resonance line by comparison with databases available at that time. From the left panel of Fig. 3 it can be seen that most of our measured ratios are located in the bottom part of the shaded area, but only measurements for cooler coronae are really consistent with solar measurements. For the 16.78/15.03 Å ratio we find solar measurements significantly higher than all our results.

The calibration used for obtaining the solar line ratios cannot be reconstructed, such that systematic uncertainties cannot be excluded as the reason for the discrepancies. However, since ratios of very nearby lines are calculated, only the relative calibration matters, which is always more accurate than the absolute calibration for such nearby lines. We point out that measurements for the Sun can also lead to different results when specific regions in the solar corona are selected, while for the stars in our sample only overall line fluxes can be obtained.

Contamination is always an issue that needs to be checked. We therefore inspected the line flux ratios of the two low-f lines at 15.27 Å and at 16.78 Å in Fig. 5, which should be independent of resonant scattering effects. This ratio is consistent with both the solar measurements and with the databases. Possible blending of the 15.27 Å line can explain the enhanced ratios measured for the cooler coronae in the left panel of Fig. 3. Such enhancements can also be identified in Fig. 5, but not for the 16.78/15.03 Å ratios.

3.2. He-like line ratio f/r

Another line ratio sensitive to resonance line scattering is the ratio f/r for He-like ions, where f is the forbidden line $^3S_1 \rightarrow {}^1S_0$ and r is the resonance line $^1P_1 \rightarrow {}^1S_0$. This ratio is also sensitive to density and temperature. Interference with density effects is not severe as Ness et al. (2002a) found low density limits for almost all stellar coronae. In Fig. 6 we plot the measured f/r ratios for O VII and Ne IX versus the luminosity contained in all three He-like lines of the respective ions, thus restricting the analysis to only the plasma regions actually emitting in the respective lines. We over-plot expected f/r ratios calculated from APEC for three temperatures $\log(T/\mathrm{K}) = 6.0$,

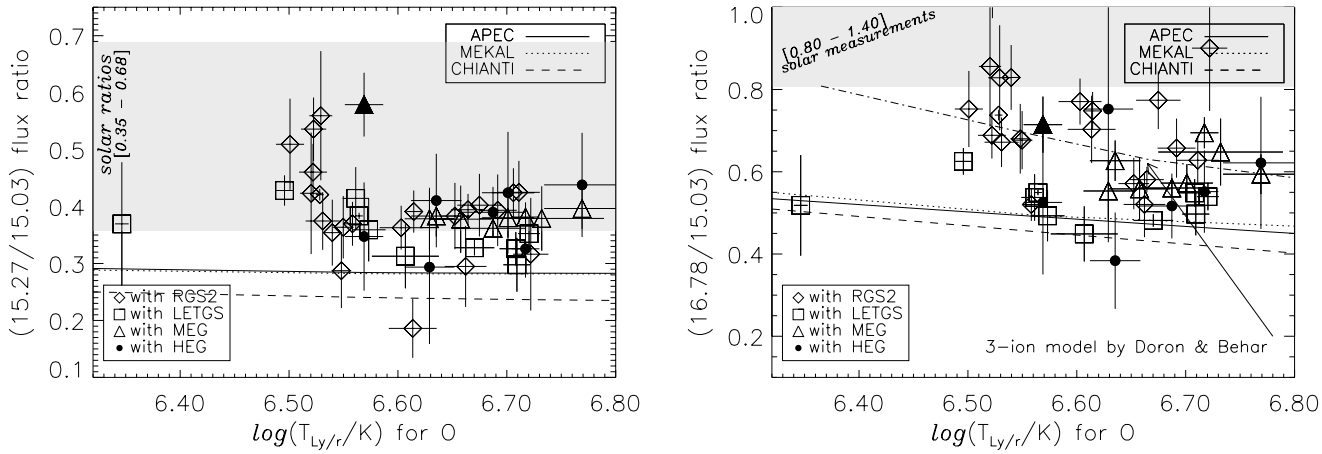

Fig. 3. Investigation of opacity effects for the Fe XVII resonance line (λ = 15.03 Å, f = 2.66) as a function of characteristic temperatures derived from O VIII/O VII (Ly_α/r) line ratios. **Left panel**: Line ratios with the Fe XVII line at 15.27 Å (f = 0.593), theoretical (low-optical depth) ratios from APEC, Chianti, and MEKAL, and solar measurements from Saba et al. (1999) (shaded area). **Right panel**: Line ratios with the Fe XVII line at 16.78 Å (f = 0.01). Same as in the left panel with additionally new calculations by Doron & Behar (2002).

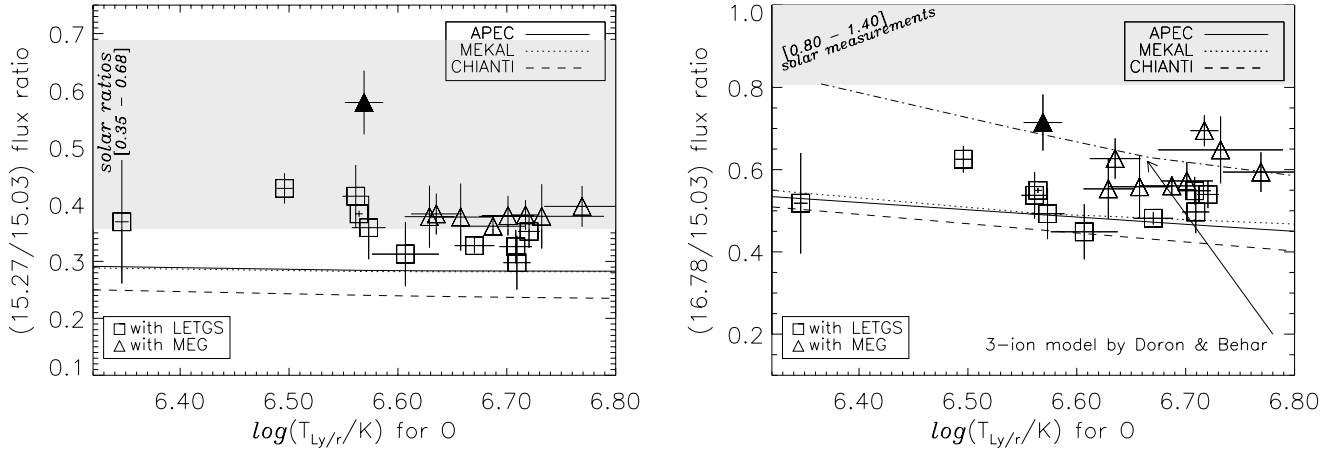

Fig. 4. Same as Fig. 3 with only the MEG and LETGS measurements. The only ratio deviating from the others is measured for EV Lac (see spectrum in Fig. 7) marked with a filled triangle.

6.3, and 6.6 assuming low densities. Good agreement between measurements and predictions can be seen. The oxygen ratios seem to generally follow the temperature trend suggested by the three theoretically predicted ratios, decreasing with increasing degree of activity. For the Ne IX f/r ratios the scatter becomes larger for the more active stars, which must be attributed to more severe blending by hotter Fe XIX lines; the blending of Ne IX by Fe XIX has been discussed by Ness et al. (2003), however, for many stars the Fe lines blending the resonance and the forbidden lines are relatively weak due to high Ne/Fe abundance ratios.

4. Discussion

One of the major aims pursued by the analysis of coronal spectra is to understand geometrical configurations of the coronal plasma. Opacity effects would make the interpretation tremendously more complicated, because assumptions about the geometrical configuration, which we want to study in the first place, would have to be made in order to account for these effects. If resonant scattering played an important role, one would naively expect that with an increasing amount of plasma these effects would become more and more visible, thus the more active stars should exhibit stronger effects on the line ratios sensitive to resonant scattering. Therefore our analysis focuses on searching for ratios of possibly optically thick resonance lines and optically thinner lines to correlate with the degree of activity.

When drawing conclusions out of the measured ratios one has to keep in mind that these ratios are not always determined by resonant scattering effects alone, but might be obstructed by other effects as, e.g., line blending or density effects. Possible temperature effects are considered quantitatively

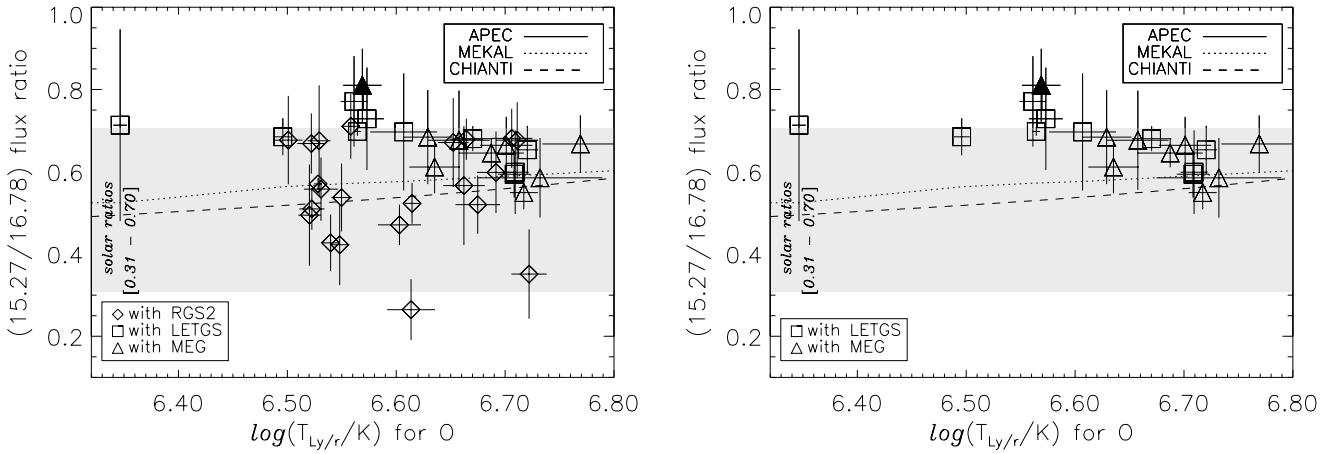

Fig. 5. Ratio of Fe XVII lines at 15.27 Å and 16.78 Å, which should not be sensitive to resonant scattering (right panel: only the MEG and LETG measurements).

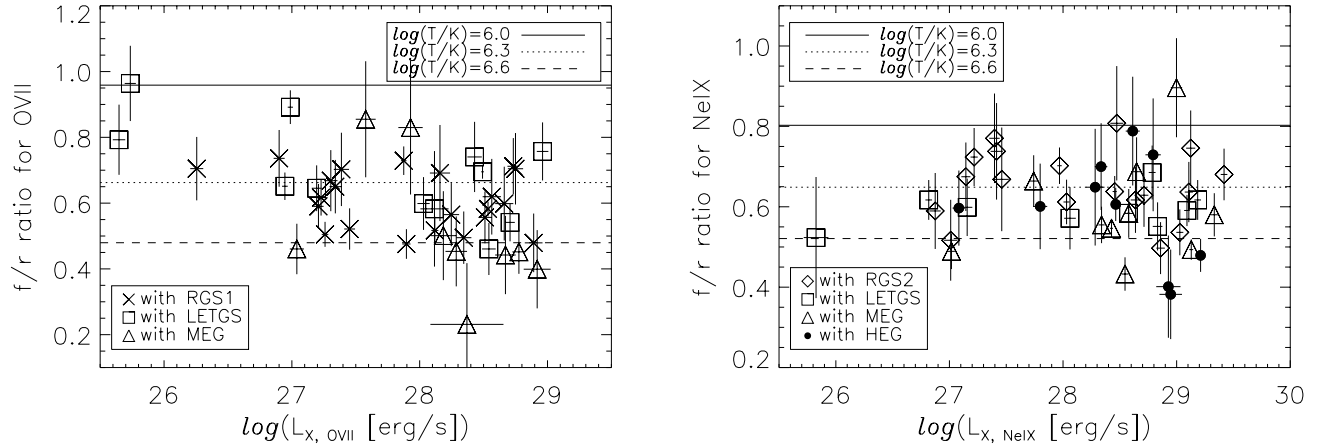

Fig. 6. He-like f/r ratio for O VII (left panel) and for Ne IX (right panel) versus the total He-like line luminosity ($r + i + f$). Measurements with RGS1, RGS2, LETGS, MEG, and HEG are compared with predictions from the APEC database for temperatures $\log(T/\mathrm{K}) = 6.0$, 6.3, and 6.6. assuming low densities.

by use of characteristic coronal temperatures derived from ratios of O VIII and O VII resonance lines.

4.1. Stellar data

Our measured ratios of Fe XVII 15.27/15.03 Å show a temperature trend indicating that enhanced line ratios are found particularly for the coolest coronae in our sample, but for the more active stars all measured line ratios scatter around a constant value of about 0.38 ± 0.07 with a slight, but insignificant increasing trend towards higher temperatures. All measured ratios are higher than predicted by the three data bases MEKAL, APEC, and Chianti, but are consistent with laboratory measurements for low optical depths obtained with EBIT. Many of the 16.78/15.03 Å line ratios are discrepant with theoretical predictions and as a sample the ratios seem generally to be discrepant with theory, but not with recent calculations by Doron & Behar (2002) that include additional processes than pure collisional excitation. No temperature trend can be seen in these data, and the scatter is much larger than for the other ratio. This scatter cannot be attributed to statistical uncertainties, because the 16.78 Å line is much stronger than the 15.27 Å line. In Fig. 4 only the ratios with the highest precision are plotted and still the 16.78 Å line seems more problematic than the ratios with the 15.27 Å line. The 16.78/15.03 Å ratio is significantly more sensitive to resonant scattering than the 15.27/15.03 Å line ratio. The larger scatter could thus represent a variety of resonant scattering processes.

The interpretation of opacity effects affecting only the 15.03 Å line (but not the 15.27 Å and the 16.78 Å lines) is certainly a possible explanation for these deviations. From the 15.27/15.03 Å ratios this would mean that opacity effects play

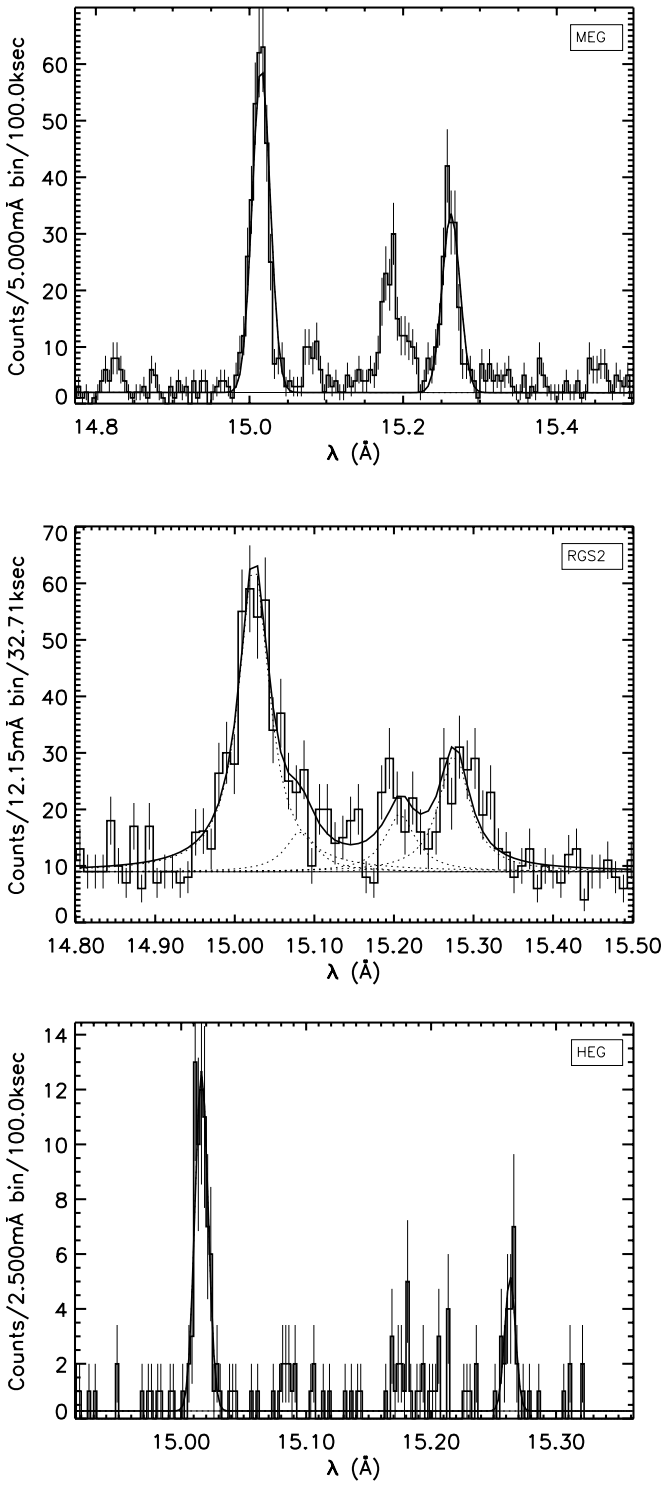

Fig. 7. Spectral region around 15 Å for EV Lac with MEG (upper panel), with the RGS2 (middle panel), and with the HEG (bottom panel). Significant differences in the 15.27 Å line compared with the 15.03 Å line can be recognized.

a larger role for the inactive stars and the Sun. However, such a temperature trend cannot be identified in the 16.78/15.03 Å line ratios lending support to the suspicion by Brown et al. (2001) about blending of the Fe XVII 15.27 Å line by an Fe XVI satellite line. However, the cited databases don't give clear indications about the nature of such a blending line, so that no clear identification can be given here. An Fe XVI satellite would disappear in the hotter coronae and leaves un-blended 15.27/15.03 Å line ratios for these coronae. Such a trend should also be visible in Fig. 5, but can only be recognized when concentrating on the LETGS and MEG measurements. From Fig. 5 we must conclude that the blending scenario cannot explain all discrepancies, unless a similar blending applies also to the 16.78 Å line.

Inspection of Fig. 4 (left panel) clearly shows that all 15.27/15.03 Å ratios measured with high confidence are systematically enhanced above the predicted ratios, but no temperature trend can be seen, neither in the data nor in the predictions. If taken at face value, these deviations suggest that the opacities are significantly non-zero for all stars, but also that optical depths are practically identical for all stars given our heterogeneous sample. Alternatively, if none of the investigated stellar coronae is optically thin, which would be quite surprising, the deviations from the databases would then have to be explained by uncertainties in the databases. For the 16.78/15.03 Å line ratio the databases agree with each other, but when using more recent calculations by Doron & Behar (2002) better agreement with our measurements can be seen. For the 15.27/15.03 Å ratio laboratory measurements disagree with the theoretical predictions. This demonstrates that the inclusion of all kinds of side effects can change theoretical predictions significantly. The ratios of the two low-f Fe XVII lines at 15.27 Å and 16.78 Å are plotted in Fig. 5 and agreement with theoretical predictions can be seen. From this it is suggestive that problems in the databases might rather lie in determining line fluxes for the 15.03 Å resonance line.

We marked the Fe XVII line ratios measured with MEG for the flare star EV Lac by filling its symbol assigned to the MEG (triangle), because in Fig. 4 this measurement is the only ratio significantly above the otherwise flat trend for the 15.27/15.03 Å ratio. In Fig. 7 we show the spectra of EV Lac obtained with MEG and RGS2 in order to demonstrate that a significant difference can already be recognized by inspecting the spectra. However, no event such as, e.g., marked flare activity during one of the observations, can be associated with such a difference. In addition the HEG spectrum shown in the bottom panel of Fig. 7 is rather consistent with the RGS2 measurement although simultaneously observed with the MEG.

Our second attempt to test for opacity effects and to probe possible other emitting regions is the ratio f/r of the He-like ions O VII and Ne IX. Although this ratio is also sensitive to density and temperature, we find roughly the same f/r ratios for all stars in our sample, definitely in agreement with plausible temperatures. No indication can be seen suggesting opacity effects from these ratios. The dependence on temperature might, however, be stronger than the sensitivity to resonant scattering effects. The f/r ratios are therefore only useful in cases of resonant scattering effects that outweigh the temperature sensitivity. For our measured ratios this means that we can exclude strong resonant scattering effects, but weaker effects could be hidden in the temperature trend.

4.2. Comparison with solar measurements

As described in Sect. 1 the discussion about opacity effects in the solar corona has been quite controversial. Since with the Sun only one star is investigated our sample of 26 stellar coronae gives more insight into trends or systematic effects. We focus on the Fe XVII line ratios, where solar measurements resulted in tempting evidence that the 15.03 Å line was significantly damped due to resonant scattering (e.g., Schmelz et al. 1997; Saba et al. 1999). Discrepancies between theoretical predictions and laboratory measurements made it difficult to identify the measured ratios as pure resonant scattering effects. In addition the MEKAL database has been upgraded since then and more refined databases have become available.

We use the most recent databases and find that the discrepancies between theoretical predictions and ratios for the Sun are still present. From the left panel of Fig. 3 it can be seen that the 15.27/15.03 Å ratios measured for the Sun are consistent with the coolest coronae in our sample but not with the hotter coronae and not with any of the more recent databases. A blending scenario for the 15.27 Å line by Fe XVI could explain the discrepancy and it would be well consistent with the temperature trend found from our sample, but it cannot be confirmed from the measured 15.27/16.78 Å line ratios. With the solar data a blending scenario could not be identified, because the temperatures encountered for the hotter coronae are never reached in the solar corona and a blending Fe XVI satellite line would thus never disappear. In the right panel of Fig. 3 the solar measurements for the 16.78/15.03 Å line ratio are all systematically higher than all the ratios from our sample as well as the predictions from the three databases MEKAL, Chianti, and APEC. The predicted ratios from Doron & Behar (2002) are consistent below $\log(T) \sim 6.5$, but most solar measurements are well above these predictions as well. Note that the discrepancies between solar ratios and our measurements are greater for the 16.78/15.03 Å ratio, which is significantly more sensitive to resonant scattering effects than the 15.27/15.03 Å ratio. Systematic uncertainties in the calibration can of course always lead to such deviations, since totally different instruments were used to obtain the solar ratios. The calibration of our instruments seem sufficiently good in order to produce similar results. If calibration errors can be excluded, a physical interpretation must be found for understanding why the Sun should be the only star where opacity effects in the corona play a role.

5. Summary and conclusions

In the solar context opacity effects in X-ray lines have been discussed controversially. In practice the strongest lines are used for the analysis rather than weaker lines, but these lines are often resonance lines and are the first candidates for opacity effects. We test for effects of resonant scattering by measuring ratios of such resonance lines and forbidden lines with significantly lower probabilities for such effects sampling many different coronae.

The Fe XVII 15.27/15.03 Å and 16.78/15.03 Å line ratios we measure systematically higher than theoretical predictions, but for all kinds of different coronae these deviations are strikingly similar. For the coolest coronae in our sample we measure 15.27/15.03 Å ratios systematically higher consistent with solar measurements of the same ratio. This trend suggests blending of the 15.27 Å line. This trend can also be seen in the 15.27/16.78 Å ratios, but only when ignoring the RGS2 measurements. In our large sample the 15.27/15.03 Å measurement for EV Lac deviates from the general trend, but an exceptional case cannot be claimed because the simultaneous HEG observation is not consistent with the MEG ratio. We interpret this measurement as a statistical outlier. For the He-like f/r ratios for oxygen and neon all ratios can be explained by reasonable temperatures, such that strong resonant scattering effects are ruled out. It cannot be excluded, that weak resonant scattering effects are hidden in the large range of ratios allowed for a reasonable temperature range.

Obviously the behavior with respect to resonant scattering is very similar for all stars in our sample. Formally one could derive optical depths τ from the measured deviations from the databases, however, similar but non-zero optical depths for stars in all kinds of stellar activity are unlikely. We therefore conclude that opacity effects should be considered as weak and undetected and uncertainties in the databases could be a more plausible explanation for the discrepancies. Since the 15.27/16.78 Å ratios are well consistent with predictions from the databases we conclude that uncertainties in the databases must lie in the 15.03 Å line.

The large discrepancies of our measurements with solar ratios are somewhat puzzling. We doubt that opacity effects play a role only for the Sun. Also the statistical argument cannot be applied in the way the EV Lac observation can be treated, since many observations for the solar corona exist. The high 15.27/15.03 Å could be explained by blending of the 15.27 Å line, because the solar coronal plasma is in the right temperature range. Possibly geometric effects might play a role. Observations of isolated emitting regions on the solar surface might exclude resonant photons from the analysis that are scattered out of not observed regions into the line of sight. Overall measurements for stars collect all photons emitted towards the observer.

The methods we chose to investigate for resonant scattering effects in coronal plasmas are commonly accepted to efficiently probe for these effects. With the amount of data gathered with the new X-ray telescopes we are convinced to operate on a sufficiently representative basis in order to decide about optical thickness of coronal plasmas in general. As to answering the question in our title we find deviations of measurements and theoretical predictions that allow the conclusion of measurable resonant scattering effects, however, we are not convinced that this conclusion is the final answer. We did find systematic deviations of line ratios from optically thin theoretical predictions, but we also found that theoretical predictions can suffer from quite some uncertainties particularly when it comes down to accounting for certain side effects. We also found striking similarities between the ratios measured for all kinds of different coronae. From the complicated geometrical configurations expected for coronal plasma optical depths are unlikely to be so similar for inactive, intermediately active, and most active coronae. The amount of emitting plasma being up to four

orders of magnitude different in X-ray luminosity raises the expectation that optical depths will be much larger for active stars than for inactive stars. The only scenario that we find plausible on the background of such similarities is that resonant scattering effects are all in the same way not detectable.

The detection of resonant scattering for the Sun seems to be a different story. We attribute these differences to some resonant scattering effects possibly always taking place. For the Sun these effects are better detectable when focusing on selected regions, while for stellar observations these effects are balanced out by observing globally. It must be pointed out that no measurement for the Sun has been reported describing any kind of "negative resonant scattering" that could balance out hypothetical global observations for the Sun.

What does it mean when we conclude resonant scattering to be taking place without being detectable for stellar coronae? Practically the analysis of stellar coronal emission always refers to globally averaged statements, not only for the aspect of resonant scattering. When analysing resonance lines the non-detectability of existent resonant scattering effects means that statements derived out of, e.g., ratios of resonance lines, made on a global basis are still valid. It has to be kept in mind that no statements can be made for individual emitting regions, but that only average conclusions about all kinds of different emitting regions can be drawn, and on this level a balance of resonant scattering effects is equivalent with negligible resonant scattering effects.

Acknowledgements. This work is based on observations obtained with XMM-Newton, an ESA science mission with instruments and contributions directly funded by ESA Member States and the USA (NASA). J.-U.N. acknowledges support from DLR under 50OR0105. MA and MG acknowledge support from the Swiss National Science Foundation (fellowship 81EZ-67388 and grant 2000-058827). The SRON National Institute for Space Research is supported financially by NWO. We thank our referee Dr. F.P. Keenan.

References

Acton, L. W. 1978, ApJ, 255, 1069
Acton, L. W., & Catura, R. C. 1976, Phil. Trans. Roy. Soc. London, 281, 383
Arnaud, M., & Rothenflug, R. 1985, A&AS, 60, 425
Audard, M., Güdel, M., Sres, A., et al. 2003, A&A, 398, 1137
Bhatia, A. K., & Saba, J. L. 2001, ApJ, 563, 434
Brown, G. V., Beiersdorfer, P., Liedahl, D. A., Widmann, K., & Kahn, S. M. 1998, ApJ, 502, 1015
Brown, G. V., Beiersdorfer, P., Chen, H., Chen, M. H., & Reed, K. J. 2001, ApJ, 557, L75
Dere, K. P., Landi, E., Young, P. R., & Del Zanna, G. 2001, ApJS, 134, 331 (Chianti)
Doron, R., & Behar, E. 2002, ApJ, 574, 518
Gabriel, A. H., & Jordan, C. 1969, MNRAS, 145, 241
Güdel, M., Guinan, E. F., & Skinner, S. L. 1997, ApJ, 483, 947
Laming, J. M., Kink, I., Takacs, E., et al. 2000, ApJ, 545, L161
Mariska, J. T. 1992, in The Solar Transition Region, Cambr. Astroph. Ser., 22 (Cambridge Univ. Press)
Mewe, R., Kaastra, J. S., & Liedahl, D. A. 1995, Legacy, 6, 16 (MEKAL)
Mewe, R., Raassen, A. J. J., Drake, J. J., et al. 2001, A&A, 368, 888
Ness, J.-U., Mewe, R., Schmitt, J. H. M. M., et al. 2001, A&A, 367, 282
Ness, J.-U., & Wichmann, R. 2002, Astron. Nachr. 323, (2002)2, 129-134 (CORA program)
Ness, J.-U., Schmitt, J. H. M. M., Burwitz, V., et al. 2002a, A&A, 394, 911
Ness, J.-U., Schmitt, J. H. M. M., Burwitz, V., et al. 2002b, A&A, 387, 1032
Ness, J.-U., Brickhouse, N. S., Drake, J. J., & Huenemoerder, D. P. 2003, ApJ, submitted
Phillips, K. J. H., Greer, C. J., Bhatia, A. K., et al. 1997, A&A, 324, 381
Phillips, K. J. H., Mathioudakis, M., Huenemoerder, D. P., et al. 2001, MNRAS, 325, 1500
Saba, J. L. R., Schmelz, J. T., Bhatia, A. K., & Strong, K. T. 1999, ApJ, 510, 1064
Schmelz, J. T., Saba, J. L. R., Chauvin, J. C., & Strong, K. T. 1997, ApJ, 477, 509
Schmitt, J. H. M. M., Drake, J. J., & Stern, R. A. 1996, A&A, 465, L51
Schrijver, C. J,, van den Oord, G. H. J., & Mewe, R. 1994, A&A, 289, L23
Smith, R. K., Brickhouse, N. S., Liedahl, D. A., & Raymond, J. C. 2001, ApJ, 556, L91
Strong, K. T. 1978, Ph.D. Thesis, Univ. London
Young, P. R., Zanna, G., Del, Landi, E., et al. 2003, ApJS, 144, 135